Plant Physiol. (1996) 112: 1055–1070

Analyzing the Light Energy Distribution in the Photosynthetic Apparatus of C_4 Plants Using Highly Purified Mesophyll and Bundle-Sheath Thylakoids[1]

Erhard Pfündel*, Elisabeth Nagel, and Armin Meister

Institut für Pflanzengenetik und Kulturpflanzenforschung, Corrensstrasse 3, D-06466 Gatersleben, Germany (E.P., E.N., A.M.); and Universität Leipzig, Institut für Botanik, Johannisallee 21, D-04103 Leipzig, Germany (E.P.)

The chlorophyll fluorescence characteristics of mesophyll and bundle-sheath thylakoids from plant species with the C_4 dicarboxylic acid pathway of photosynthesis were investigated using flow cytometry. Ten species with the NADP-malic enzyme (NADP-ME) biochemical type of C_4 photosynthesis were tested: *Digitaria sanguinalis* (L.) Scop., *Euphorbia maculata* L., *Portulaca grandiflora* Hooker, *Saccharum officinarum* L., *Setaria viridis* (L.) Beauv., *Zea mays* L., and four species of the genus *Flaveria*. This study also included three species with NAD-ME biochemistry (*Atriplex rosea* L., *Atriplex spongiosa* F. Muell., and *Portulaca oleracea* L.). Two C_4 species of unknown biochemical type were investigated: *Cyperus papyrus* L. and *Atriplex tatarica* L. Pure mesophyll and bundle-sheath thylakoids were prepared by flow cytometry and characterized by low-temperature fluorescence spectroscopy. In pure bundle-sheath thylakoids from many species with C_4 photosynthesis of the NADP-ME type, significant amounts of photosystem II (PSII) emission can be detected by fluorescence spectroscopy. Simulation of fluorescence excitation spectra of these thylakoids showed that PSII light absorption contributes significantly to the apparent excitation spectrum of photosystem I. Model calculations indicated that the excitation energy of PSII is efficiently transferred to photosystem I in bundle-sheath thylakoids of many NADP-ME species.

Plant species with the C_4 dicarboxylic acid pathway of photosynthesis probably evolved from C_3 ancestors in response to decreasing atmospheric CO_2 concentrations (Hatch, 1992; Hattersley and Watson, 1992). In C_3 photosynthesis, fixation of atmospheric CO_2 and its subsequent reduction to carbohydrates is associated with reactions of the Calvin cycle occurring in chloroplasts in leaf mesophyll. In C_4 photosynthesis, the Calvin cycle is confined to cells surrounding the vascular bundles in leaves, the so-called bundle-sheath cells. Fixation of atmospheric CO_2 takes place in cells interposing bundle-sheath cells and epidermis, the mesophyll cells.

In C_4 plants, CO_2 fixation results in formation of C_4 acids that are transported into the bundle-sheath compartment, where CO_2 is released and introduced into the Calvin cycle. Currently, three biochemical types of C_4 photosynthesis are distinguished (Hatch, 1987). Here, we focus on two types, C_4 photosynthesis with NADP-ME chemistry and C_4 photosynthesis with NAD-ME chemistry.

In NADP-ME species, the primary product of CO_2 fixation is oxaloacetate, which is reduced to malate in mesophyll chloroplasts and transferred to the bundle-sheath compartment. The release of CO_2 in bundle-sheath chloroplasts regenerates the NADPH consumed during oxaloacetate reduction in mesophyll cells. The transfer of NADPH, which is implied by malate transport, along with the transfer of a reduced Calvin cycle intermediate (dihydroxyacetone phosphate) can account for most of the redox equivalents required for carbon reduction in bundle-sheath chloroplasts (Hatch, 1987).

The ATP required to drive the Calvin cycle can be formed in the absence of PSII by cyclic electron transport via PSI. This is supported by the fact that the activity of PSII is low compared with PSI in bundle-sheath chloroplasts (Edwards and Walker, 1983; Hatch, 1987). Similar activities for both photosystems exist in mesophyll chloroplasts.

In contrast to NADP-ME photosynthesis, in the mesophyll cells of NAD-ME species oxaloacetate is first converted into aspartate, which is then shuttled into the bundle-sheath compartment, where CO_2 is released by the mitochondria (Hatch, 1987). Here, the mesophyll-to-bundle-sheath transport of fixed CO_2 does not imply concomitant transfer of NADPH. By assuming mesophyll-to-bundle-sheath transfer of dihydroxyacetone phosphate with NADPH-dependent regeneration of the molecule in mesophyll chloroplasts, Hatch (1987) estimated that equal amounts of NADPH were consumed in both compartments to fix CO_2. This is consistent with the fact that PSI and PSII activities were roughly comparable in mesophyll and bundle-sheath chloroplasts (Edwards and Walker, 1983; Hatch, 1987).

Because conflicting data on PSII activity has been reported, the degree of PSII deficiency in bundle-sheath chloroplasts of NADP-ME species has always been a matter of debate (Edwards and Walker, 1983; Hatch, 1987). Edwards and Walker (1983) have argued that the discrepancy could be due either to different experimental assay conditions or

[1] This work was supported by the Deutsche Forschungsgemeinschaft (Me 1083/1–2).

* Corresponding author; e-mail erhard@magicalf.boerde.de; fax 49–39482–5139.

Abbreviations: Chl, chlorophyll; LHCI, light-harvesting complex of PSI; LHCII, light-harvesting complex of PSII; NAD-ME, NAD-malic enzyme; NADP-ME, NADP-malic enzyme.

to cross-contamination of the bundle-sheath with the mesophyll chloroplasts. The situation has become more complex, since recent immunological studies indicated that PSII with an inactive reaction center is present in NADP-ME bundle-sheath chloroplasts (Höfer et al., 1992; Meierhoff and Westhoff, 1993; Bassi et al., 1995).

In this contribution we address the issue of whether a functioning PSII exists in chloroplasts of C_4 plants by using a recently developed flow cytometric method (Pfündel and Meister, 1996). Flow cytometry overcomes the uncertainties of cross-contamination by sorting pure mesophyll and bundle-sheath thylakoids from chloroplast preparations obtained by conventional procedures. This method permits routine preparation of highly pure chloroplast fractions at quantities suited for detailed spectroscopic analysis of Chl fluorescence.

Here, we demonstrate the presence of PSII in bundle-sheath thylakoids from various NADP-ME species. In these thylakoids, excitation of PSII appears to be effectively drained off by PSI so that significant PSII activity can be ruled out.

MATERIALS AND METHODS

An overview of the species investigated is presented in Table I. The table also includes the biochemical type of C_4 photosynthesis for all species except *Cyperus papyrus* and *Atriplex tatarica*, for which we were unable to locate references specifying their biochemical type. Closely related species of *C. papyrus* always exhibit NADP-ME-type photosynthesis (Bruhl et al., 1987) and *C. papyrus* was similar to the NADP-ME species, *Zea mays*, in the flow cytometric analysis presented here. Thus, we will provisionally classify *C. papyrus* as an NADP-ME species. Flow cytometric results of *A. tatarica* resembled those of the NAD-ME species *Atriplex rosea*, so *A. tatarica* is classified along with the NAD-ME species.

Table I. *Summary of the plant species investigated*

Species are ordered according to fluorescence characteristics detected by flow cytometry (compare Fig. 2B). Characters in the left column identify individual species in Figures 2, 3, and 6. Information on the biochemical type of C_4 photosynthesis is given with references.

Species	Biochemical Type
Cyperus papyrus L.	C_4, no biochemical type specified, 10 species of *Cyperus* subgen. *Cyperus* classified as NADP-ME (Bruhl et al., 1987)
Zea mays L.	NADP-ME (Mateu-Andrés, 1993)
Euphorbia maculata L.	NADP-ME (Mateu-Andrés, 1993)
Saccharum officinarum L.	NADP-ME (Mateu-Andrés, 1993)
Digitaria sanguinalis (L.) Scop.	NADP-ME (Mateu-Andrés, 1993)
Setaria viridis (L.) Beauv.	NADP-ME (Mateu-Andrés, 1993)
Portulaca grandiflora Hooker	NADP-ME (Brown, 1977)
Flaveria trinervia (Spreng.) C. Mohr	NADP-ME (Moore et al., 1989)
Flaveria palmeri J.R. Johnson	NADP-ME C_4-like (Moore et al., 1989)
Flaveria australasica Hook	NADP-ME (Moore et al., 1989)
Flaveria bidentis (L.) Kuntze	NADP-ME (Moore et al., 1989)
Portulaca oleracea L.	NAD-ME (Mateu-Andrés, 1993)
Atriplex spongiosa F. Muell.	NAD-ME (Moore et al., 1984)
Atriplex rosea L.	NAD-ME (Mateu-Andrés, 1993)
Atriplex tatarica L.	C_4, no biochemical type specified (Mateu-Andrés, 1993)

All plants were cultivated in the greenhouse. *C. papyrus* and *Saccharum officinarum* were grown from rootstock during the spring and summer. All other plant species were propagated from seeds on garden mulch in pots during various seasons. From October through April, supplementary light of 150 to 200 $\mu E\ m^{-2}\ s^{-1}$ intensity at leaf level was given from 6 AM until 10 PM. The light source was a 400-W high-pressure sodium lamp (SON-T AGRO 400, Phillips, Brussels, Belgium) mounted 160 cm above ground. For chloroplast isolation, fully developed leaves that had been dark-adapted overnight were used.

Chloroplast Isolation

Mesophyll and bundle-sheath chloroplasts were obtained by conventional procedures for all of the plant species listed in Table I, as described for *Flaveria trinervia* by Höfer et al. (1992) with the modifications specified by Pfündel and Meister (1996).

For mesophyll preparation, leaves were homogenized in a blender (model HO4, E. Bühler, Bodelshausen, Germany) at 6000 rpm for 30 s. Chloroplasts released by this procedure were separated from nonhomogenized material by filtration and collected by centrifugation.

Bundle-sheath chloroplasts were isolated from leaf tissue retained by the filtration above. The material was homogenized at 26,000 rpm for 30 to 60 s and enzymatically digested with 1% (w/v) cellulase (Onozuka R-10) and 0.2% (w/v) Macerozyme R10 (both Serva, Heidelberg, Germany) at 27°C for 45 to 60 min. The enzymatically treated tissue was homogenized (10,000 rpm for 20 s) and then filtrated. Chloroplasts of the filtrate were collected by centrifugation.

Pellets resulting from mesophyll or bundle-sheath chloroplast preparations were diluted to a Chl $a+b$ concentration of 1 mM with a storage medium containing 60% (v/v) glycerin. Preparations were kept in liquid nitrogen until flow cytometric analysis. Since freezing affects the integrity of the chloroplast envelope membrane (Heber et al., 1981, and refs. therein), all chloroplast preparations are referred to as "thylakoids" in this study.

Flow Cytometry

Prior to flow cytometry, thylakoid membranes were diluted with 5 mM Hepes (KOH), pH 8.0, to a Chl $a+b$ concentration of 50 μM. Flow cytometrical analysis and particle sorting was done with a sorting flow cytometer (FACStar^{Plus}, Becton Dickinson) as described in detail by Pfündel and Meister (1996). Flow cytometry allows the analysis of individual chloroplasts according to their fluorescence characteristics. In the flow cytometer used, a string of single particles is generated by injecting thylakoid suspension into a fluid stream, which then passes through

a nozzle. Excitation of Chl fluorescence occurred 0.25 mm below the nozzle tip with 488-nm light from an argon ion laser (INNOVA 90–5, Coherent, Palo Alto, CA) operated at 500 mW of output power.

Chl fluorescence was separated into short and long wavebands by a cold mirror (645 FK 84–25, LOT-Oriel, Darmstadt, Germany), which at 45° preferably reflects light below 700 nm and transmits light above 700 nm. The short-wavelength fluorescence was further confined to the range of 645 to 700 nm by a combination of one short- and one long-pass filter (700 FL 07–25, LOT-Oriel, and RG 645, Schott, Mainz, Germany, respectively). The long-wavelength fluorescence was delimited by a long-pass filter (RG 715, Schott).

Short- and long-wavelength fluorescence were detected simultaneously with two red-sensitive photomultiplyer tubes (R 1477, Hamamatsu, Toyooka, Japan). We classified thylakoids by the ratio of short- to long-wavelength fluorescence. This parameter is used as the abscissa in the flow cytometric histograms of Figure 1.

For sorting of mesophyll and bundle-sheath thylakoids, the nozzle vibrates at 15 kHz, which causes the sample beam to separate into droplets 5 mm after the point of fluorescence excitation. Depending on the short-to-long-wavelength fluorescence ratio of thylakoids, the droplets were positively or negatively charged and directed into test tubes by the field of a capacitor. Only droplets containing one particle were sorted; empty droplets or droplets containing more than one particle were discarded. In this paper, we denote the mesophyll and bundle-sheath thylakoids purified by flow cytometry as pure mesophyll and pure bundle-sheath thylakoids, respectively.

Fluorescence Spectroscopy

Fluorescence spectra were recorded at 77 K with a fluorimeter (model LS 50B, Perkin-Elmer) using a scan speed of 6.7 nm s^{-1}. For emission spectra, bandwidths of excitation and emission were 15 and 4 nm, respectively. Excitation spectra were recorded using a 4-nm excitation bandwidth and a 15-nm emission bandwidth. Filter combinations to reduce stray light and correction of spectral distortion in excitation spectra were as described by Pfündel and Meister (1996).

For fluorescence spectroscopy, thylakoids purified by flow cytometry and suspended in buffer (FACSFlow, Becton Dickinson) were diluted with 100% glycerin (1:1, v/v). The Chl concentrations in these samples were less than or equal to 1 μM. Samples were placed in quartz tubes of 1-mm inner diameter (Heralux tubes, Hellma, Müllheim, Germany), and measured in the low-temperature sample holder of the fluorimeter.

Fluorescence reabsorption as determined by low-temperature fluorescence spectroscopy (compare Weis, 1985) was negligible under these conditions. The low signal-to-noise ratio at low Chl concentrations was reduced by averaging between 4 and 32 spectral scans. In emission spectra, stray light became significant. These artifacts were corrected by subtracting a baseline taken from pure, frozen solvent. Data handling and curve fitting were with scientific graphing software (SigmaPlot, Jandel Scientific, Erkrath, Germany).

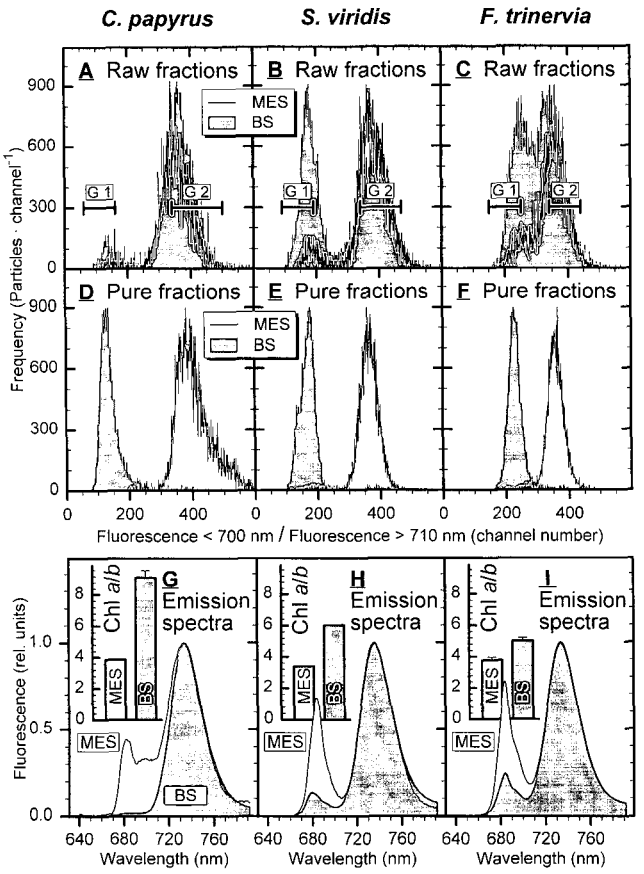

Figure 1. Histograms, fluorescence emission spectra, and Chl *a/b* ratios of thylakoids from *C. papyrus*, *S. viridis*, and *F. trinervia*. Data of *C. papyrus* are shown in the left panels. Results obtained with *S. viridis* and *F. trinervia* are displayed in the center and right panels, respectively. In all panels, data of mesophyll thylakoids (MES) are drawn in the foreground (transparent), and those of bundle-sheath thylakoids (BS) are drawn in the background (gray). A to F contain histograms obtained by flow cytometry. In these panels, the abscissa is the fluorescence intensity of individual particles at wavelengths <700 nm relative to the fluorescence intensity at wavelengths >710 nm (see "Materials and Methods"). The ordinate is the frequency with which a particular fluorescence ratio occurred. A to C show data from mesophyll and bundle-sheath thylakoids isolated by conventional procedures. In the latter panels, the horizontal bars (labeled G1 and G2) indicate the gates of fluorescence ratios chosen for sorting of pure bundle-sheath and mesophyll thylakoids. Histograms of thylakoids purified by flow cytometry are shown in D to F. G to I give the 77-K fluorescence emission spectra of pure thylakoids. Chl *a/b* ratios are shown as insets. Chl *a/b* ratios correspond to the mean of at least three determinations. SD values are indicated as vertical bars.

Chl a/b ratios were determined fluorimetrically by the method of Meister (1992) with modifications as described by Pfündel and Meister (1996).

RESULTS

Flow Cytometry

Using flow cytometry, we analyzed mesophyll and bundle-sheath thylakoids obtained by conventional iso-

lation procedures from 15 different plant species with C_4 photosynthesis. To illustrate the patterns of the results observed in NADP-ME species, we chose *C. papyrus*, *Setaria viridis*, and *Flaveria trinervia* (Fig. 1, A–C). Flow-cytometry-derived histograms of conventionally prepared mesophyll thylakoids always contained two peaks, which implies the existence of two types of particles. The major peak was located at higher short-to-long-wavelength fluorescence-intensity ratios than the minor peak. Among NADP-ME species, the relative size of the minor population varied inconsistently and was smallest for *C. papyrus*.

The conventionally prepared bundle-sheath thylakoids from NADP-ME species also consisted of two particle populations. Their positions corresponded with the histogram peaks of mesophyll thylakoids (Fig. 1, A–C). As with mesophyll thylakoids, the relative size of the two histogram peaks varied (Fig. 1, A–C). In all NADP-ME species, the population with low short-to-long-wavelength fluorescence-intensity ratios was significantly enriched in conventionally prepared bundle-sheath thylakoids compared with conventionally prepared mesophyll thylakoids. In *C. papyrus*, *S. viridis*, and *F. trinervia*, the relative increase was estimated to be 3-, 6-, and 4-fold, respectively (Fig. 1, A–C).

The results obtained in C_4 species with NAD-ME biochemistry differed from those in NADP-ME species. The conventionally isolated mesophyll thylakoids did not exhibit two distinct particle populations; instead, one major peak with a shoulder located at increased fluorescence ratios was observed (not shown). In marked contrast to NADP-ME species, the conventionally prepared bundle-sheath thylakoids contained more particles at high short-to-long-wavelength fluorescence ratios compared with mesophyll thylakoids (not shown).

Within NADP-ME species, the location of histogram peaks relative to each other varied. Clear separation of the two peaks was observed for *C. papyrus* (Fig. 1A). Smaller differences were found among species of the genus *Flaveria*, represented by *F. trinervia* in Figure 1C. *S. viridis* exhibited an intermediate separation of the peak positions (Fig. 1B). In the additional NADP-ME species investigated, distances between histogram peaks ranged between the results of *C. papyrus* and those of *F. trinervia* (histograms not shown).

Also among NAD-ME species, the relation between peaks observed in conventionally prepared mesophyll and bundle-sheath thylakoids varied (histograms not shown). In *A. tatarica* and *A. rosea* two particle populations were apparent in histograms, where the distance between peak positions was comparable to the distance in *F. trinervia*. In comparison the peaks in *Atriplex spongiosa* and *Portulaca oleracea* were much closer.

To obtain pure mesophyll and bundle-sheath thylakoids, particles were sorted by flow cytometry. Typical ranges of short-to-long-wavelength fluorescence ratios used to sort particles are presented as horizontal bars in Figure 1, A to C. When the two thylakoid populations were clearly separated, ranges were set to include most of the short-to-long-wavelength fluorescence ratios of histogram peaks (Fig. 1, A and B). Depending on the overlap of populations, both sorting gates were moved to the edge regions of the histogram to avoid cross-contamination (Fig. 1C).

In NADP-ME and NAD-ME species, we denote the particles sorted from the major peak of conventionally prepared mesophyll thylakoids as pure mesophyll thylakoids. Particles derived from peaks increased by the conventional method for preparing bundle-sheath thylakoids will be called pure bundle-sheath thylakoids. Typical histograms of pure mesophyll and bundle-sheath thylakoids are given in Figure 1, D to F. Overlap of pure thylakoid fractions was also negligible in the other species investigated.

Flow Cytometry and Fluorescence Emission Spectra

Low-temperature emission spectra of Chl fluorescence were recorded from pure mesophyll and pure bundle-sheath thylakoids. As in the previous section, *C. papyrus*, *S. viridis*, and *F. trinervia* were chosen to demonstrate typical results of NADP-ME species (Fig. 1, G–I). With the exception of bundle-sheath thylakoids of *C. papyrus*, two major emission bands were observed for all thylakoids from the NADP-ME species. One was located in the spectral range of 680 to 684 nm and the other between 734 and 736 nm. Similar emission-band positions were found in NAD-ME species (not shown).

Pure bundle-sheath thylakoids from NADP-ME species showed significant variations in the ratio of short-to-long-wavelength emission. In *C. papyrus* the short-wavelength fluorescence was close to zero, whereas in *F. trinervia* the maximum value at short wavelengths was 24% of the long-wavelength band (Fig. 1, G and I). In *S. viridis*, the relative size of the short-wavelength peak was 14%. In pure mesophyll thylakoids of NADP-ME species, ratios of emission peaks differed (compare Fig. 1, G–I). The relative differences between species were less pronounced in pure mesophyll thylakoids than in pure bundle-sheath thylakoids.

For all species, we examined the relationship between short-to-long-wavelength fluorescence ratios of pure thylakoids and the fluorescence ratios as revealed by the peak positions in flow cytometric histograms of conventionally isolated thylakoids. To quantify fluorescence ratios with flow cytometry, the absolute positions of histogram peaks are inappropriate because flow cytometer settings vary between experiments and species. Since the instrument settings were constant for individual species, we used the mesophyll-to-bundle-sheath ratio of histogram peak positions to characterize fluorescence ratios. This parameter is used as the abscissa in Figure 2. The calculations yielded values between 1.2 and 3.2 for NADP-ME species and <1 for NAD-ME species.

Low-temperature emission spectra of pure thylakoids were analyzed in an analogous fashion. Total short-wavelength fluorescence was calculated by integrating the spectrum between the starting wavelength and the upper spectral limit of the short-wavelength fluorescence window of the flow cytometry (700 nm). The lower limit of the long-wavelength window (710 nm) was used to obtain total long-wavelength fluorescence from emission spectra. For all samples, the short-to-long-wavelength ratio of emission

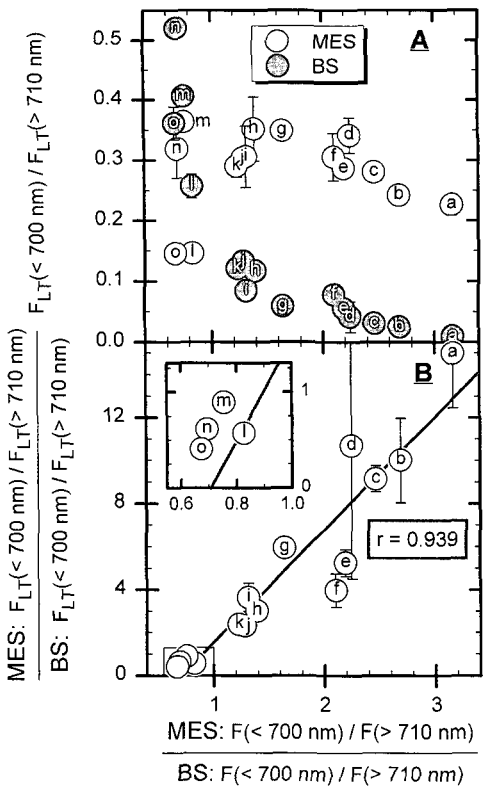

Figure 2. Relationship between fluorescence emission and peak positions in the histograms of 15 species with C_4 photosynthesis. Labeling of data points (a through o) identify individual species, as specified in Table I. In A, short-to-long-wavelength fluorescence ratios derived from 77-K emission spectra (ordinate) of pure mesophyll (open symbols) and bundle-sheath thylakoids (filled symbols) are plotted against relative peak positions in histograms of conventionally prepared thylakoids (abscissa). Relative peak positions correspond to the position of mesophyll thylakoids relative to the position of bundle-sheath thylakoids (see "Results"). The same abscissa are used in A and B. In B, short-to-long-wavelength fluorescence of 77-K emission spectra of mesophyll thylakoids is expressed relative to the corresponding fluorescence ratio in bundle-sheath thylakoids. Nonlabeled data points are shown with magnified scales in the inset. Means of three to five fluorescence measurements are given. SD values are indicated by bars (when bars are omitted, the SD is smaller than the dot radius). Linear regression (straight line) is calculated to all data points in B. The correlation coefficient (r) is 0.939.

spectra is plotted against the relative histogram peak ratios in Figure 2A. From fluorescence ratios of emission spectra of Figure 2A, mesophyll-to-bundle-sheath ratios were calculated and are plotted versus the equivalent histogram ratios in Figure 2B.

Figure 2A shows that in all NADP-ME species, the relative short-wavelength fluorescence in emission spectra was higher in pure mesophyll than in pure bundle-sheath thylakoids, and vice versa in NAD-ME species. In pure bundle-sheath thylakoids of NADP-ME species, the relative short-wavelength emission was lowest in *C. papyrus* and highest in the species of the genus *Flaveria* (Fig. 2A). Figure 2B demonstrates the linear relationship between data from fluorescence spectroscopy and those from flow cytometry.

Relationship between Fluorescence Emission Spectra and Chl *a/b* Ratios

Chl a/b ratios of pure mesophyll and bundle-sheath thylakoids are shown as insets in Figure 1, G to I, for *C. papyrus*, *S. viridis*, and *F. trinervia*, respectively. For pure thylakoid fractions from all species, Chl a/b ratios are plotted against the short-to-long-wavelength fluorescence ratios of emission spectra in Figure 3A.

A hyperbolic relationship between pigment ratios and fluorescence ratios was obtained (Fig. 3A). The highest Chl a/b value was observed in bundle-sheath thylakoids of *C. papyrus*, the thylakoid fraction exhibiting the lowest short-wavelength fluorescence. Generally, high ratios of Chl a/b were found in samples with low short-to-long-wavelength

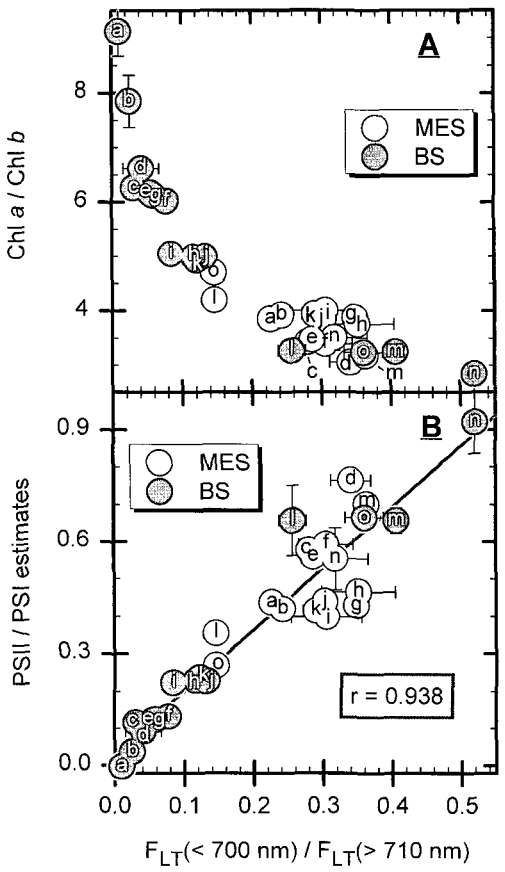

Figure 3. Relationship between Chl a/b ratios and fluorescence emission. Data of pure mesophyll (open dots) and pure bundle-sheath thylakoids (filled dots) for 15 species with C_4 photosynthesis are shown (see Table I for identification of individual species). In A, Chl a/b ratios are plotted against the ratio of short-to-long-wavelength area of 77-K emission spectra taken from Figure 2A. In B, ordinate values are estimated ratios of PSII to PSI. Estimates were derived from Chl a/b ratios as specified in "Appendix." Means of three to five measurements are given. SD values are shown as bars (not shown when their values are smaller than the dot radius). The straight line in B was obtained by linear regression (r = 0.938).

fluorescence ratios, i.e. bundle-sheath thylakoids from NADP-ME species. Mesophyll thylakoids from *A. tatarica* and *P. oleracea* were similar to bundle-sheath thylakoids of *Flaveria* species. All other samples exhibited lower Chl *a*/*b* ratios and higher fluorescence ratios.

Within NADP-ME species, Chl *a*/*b* values were higher in bundle-sheath thylakoids than in mesophyll thylakoids. In *A. spongiosa*, similar Chl *a*/*b* ratios were observed for both types of thylakoids. In all other NAD-ME species, Chl *a*/*b* was lower in bundle-sheath thylakoids than in the mesophyll thylakoids. The differences between mesophyll and bundle-sheath thylakoids were less pronounced in NAD-ME species than in NADP-ME species.

From Chl *a*/*b* values, we derived estimates of the PSII-to-PSI ratio using the simple model described in "Appendix." The model yielded estimates that were linearly correlated to the short-to-long-wavelength fluorescence ratios derived from fluorescence spectroscopy (Fig. 3B).

Fluorescence Excitation Spectra

The excitation spectra of pure mesophyll and bundle-sheath thylakoids of all species were determined at the 685- and 735-nm emission wavelengths. Again, the species *C. papyrus*, *S. viridis*, and *F. trinervia* were chosen to demonstrate typical original traces (Fig. 4). In thylakoids of all species, excitation spectra showed two distinct maxima, one in the range of 430 to 440 nm and one between 470 and 480 nm. In samples with very low short-wavelength emission, the excitation spectra at the 685-nm emission wavelength were noisy. This was the case in bundle-sheath thylakoids of *C. papyrus* (Fig. 4D). Noisy 685-nm excitation spectra were also obtained with bundle-sheath thylakoids of *Z. mays* and *Euphorbia maculata* (spectra not shown).

Fluorescence excitation spectra of all samples were classified by the ratio of their value at the 475-nm excitation wavelength to the 435-nm maximum. Calculations yielded values <1 in all cases (Fig. 5). In all samples except for the bundle-sheath thylakoids isolated from *E. maculata*, the excitation spectra at the 685-nm emission wavelength exhibited higher 475-nm excitation than excitation spectra at the 735-nm emission wavelength.

Within bundle-sheath thylakoids of NADP-ME species, the relative 475-nm values in excitation spectra at 735-nm emission tended to increase with increasing short-wavelength emission in fluorescence emission spectra. High 475-nm excitation was found in species of *Flaveria* (Fig. 5B), which also showed significant short-wavelength fluorescence emission (Fig. 2A). The lowest values for 475-nm excitation were obtained in the two species with the lowest short-wavelength emission, i.e. *C. papyrus* and *Z. mays*. *E. maculata* was exceptional in that its 475-nm excitation value was similar to those of *F. trinervia* and *Flaveria australasica* (Fig. 5B), whereas its ratio of short-to-long-wavelength fluorescence emission was comparable to that of *Z. mays* (Fig. 2A). For bundle-sheath thylakoids of all NADP-ME species except *E. maculata*, we obtained a linear relation between the relative 475-nm value in 735-nm excitation spectra and the short-to-long-wavelength ratio of fluorescence emission spectra (Fig. 6).

Deconvolution of Fluorescence Excitation Spectra

The apparent excitation spectra of 735-nm fluorescence ($F_{735}[\lambda ex]$) was resolved into PSI and PSII components according to:

$$F_{735}(\lambda ex) = Fc1 \times e_{PS1}(\lambda ex) + Fc2 \times e_{PS2}(\lambda ex)$$

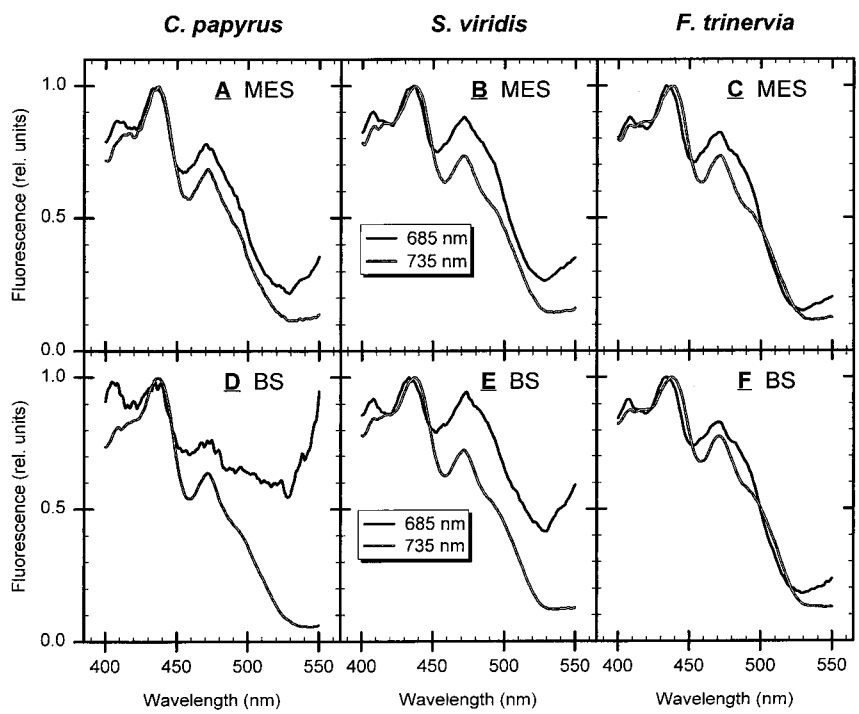

Figure 4. Fluorescence excitation spectra of thylakoids purified by flow cytometry. Normalized excitation spectra of 77-K fluorescence of *C. papyrus* are shown in A and D, of *S. viridis* in B and E, and of *F. trinervia* in C and F. Graphs of mesophyll (MES) and bundle-sheath thylakoids (BS) are depicted in the upper and lower panels, respectively. In all panels, excitation spectra of 685-nm fluorescence are drawn as black lines. Gray lines are excitation spectra of 735-nm fluorescence.

where $e_{PS1}(\lambda ex)$ and $e_{PS2}(\lambda ex)$ represent excitation spectra of pure PSI and PSII, respectively, normalized to equal values at 435 nm. *Fc*1 and *Fc*2 are free parameters that were determined by fitting the sum of PSI and PSII components to $F_{735}(\lambda ex)$.

For all spectral simulations, the excitation spectrum of 735-nm fluorescence of bundle-sheath thylakoids from *C. papyrus* (Fig. 4D) was used as the PSI spectrum, $e_{PS1}(\lambda ex)$. This spectrum was chosen because PSII emission was virtually absent in these thylakoids (Fig. 1G). The excitation spectrum of 685-nm fluorescence of the sample under investigation was utilized as the PSII component, $e_{PS2}(\lambda ex)$.

For mesophyll and bundle-sheath thylakoids from *C. papyrus*, *S. viridis*, and *F. trinervia*, the results of spectral simulations were compared with apparent excitation spectra at 735-nm emission and are shown in Figure 7. Generally, the relative peak size and the shape of calculated spectra agreed well with experimental traces. In some samples, the simulated spectrum deviated from the measured one, as is illustrated by spectra of *F. trinervia* presented in Figure 7, C and F. Deviations occurred in the region from 490 to 530 nm and were accompanied by a slight blue-shift of the absolute maximum of the calculated spectrum compared to $F_{735}(\lambda ex)$.

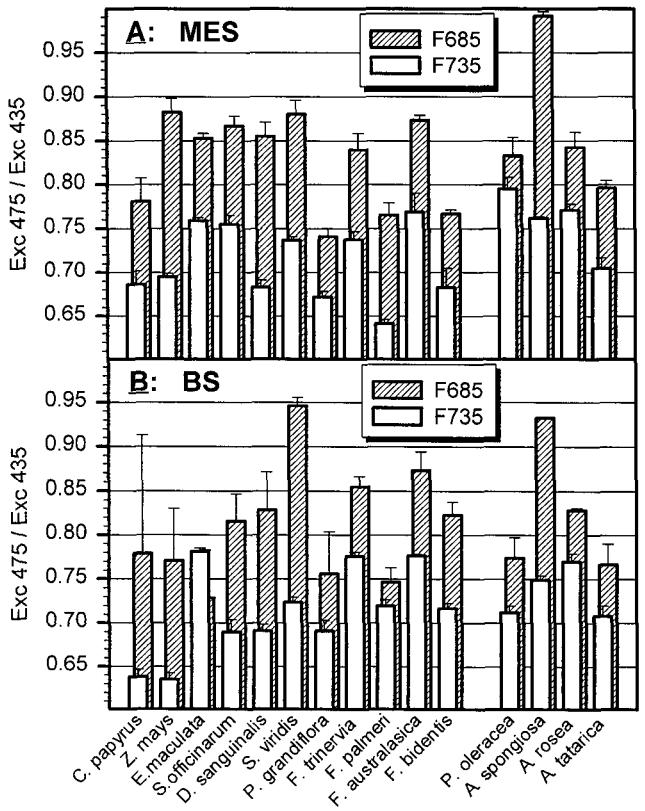

Figure 5. Relative values of the 475-nm maximum in fluorescence excitation spectra. Data correspond to the value at 475-nm divided by the 435-nm value of 77-K fluorescence excitation spectra. Excitation spectra were recorded with 685-nm (open columns) and 735-nm (hatched columns) emission wavelengths. Results of mesophyll and bundle-sheath thylakoids purified by flow cytometry are given in A and B, respectively. Individual species are identified by abscissa labels in B. Means of three to five measurements (± SD) are given.

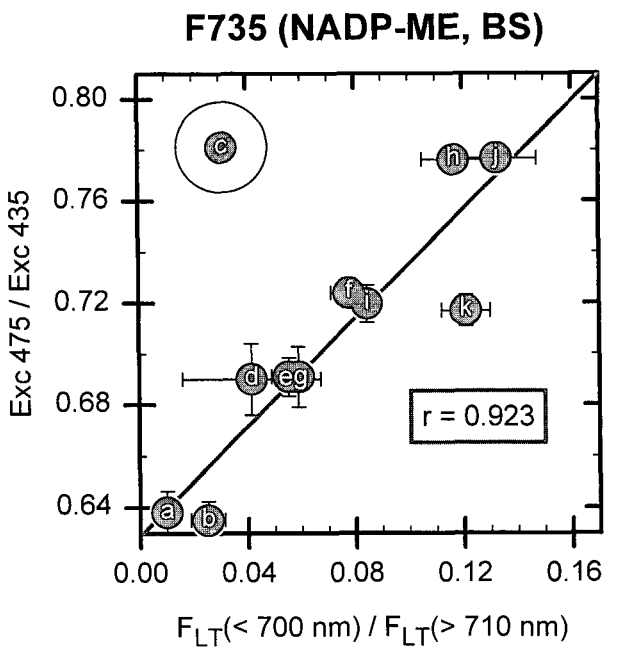

Figure 6. Relationship between excitation and emission spectra. The results of pure bundle-sheath thylakoids of NADP-ME species are shown. Normalized 475-nm values of excitation spectra of 735-nm fluorescence (taken from Fig. 5B) are plotted against the short-to-long-wavelength area ratio of 77-K emission spectra (taken from Fig. 2A). Means of three to five measurements are given ± SD values. Linear regression (straight line) was calculated without *E. maculata* (circled data point). The correlation coefficient (r) = 0.923.

For all species, the contribution of PSII absorption to $F_{735}(\lambda ex)$ was quantified by quotients of *Fc*2/*Fc*1 (Fig. 8A). The value of *Fc*2/*Fc*1 was 0 in bundle-sheath thylakoids from *C. papyrus* and close to 0 in bundle-sheath thylakoids of *Z. mays*. The highest PSII contributions were obtained with mesophyll thylakoids from *P. oleracea* and bundle-sheath thylakoids from *A. rosea* (*Fc*2/*Fc*1 > 1.4).

Within bundle-sheath thylakoids of NADP-ME species, the pattern of *Fc*2/*Fc*1 resembled the trend observed for the 475-nm band in excitation spectra at 735-nm emission (compare Figs. 8A and 5B). The relationship between the value of *Fc*2/*Fc*1 in mesophyll thylakoids and the value of *Fc*2/*Fc*1 in bundle-sheath thylakoids varied inconsistently for the individual species.

We calculated relative quantum yields of energy transfer from PSII to PSI (Φ_T) by employing the model described in the Appendix. We needed the quotients *Fc*2/*Fc*1 and PSI-to-PSII ratios as estimated from Chl *a*/*b* values to input to the model.

In mesophyll thylakoids of NADP-ME species, the relative quantum yields for energy transfer ranged between 0.30 (*Flaveria palmeri*) and 2.11 (*F. australasica*) (Fig. 8B). In all NADP-ME species except *C. papyrus* and *Z. mays*, relative quantum yields in bundle-sheath thylakoids were markedly higher than in mesophyll thylakoids. In contrast to the trend observed for NADP-ME photosynthesis, the

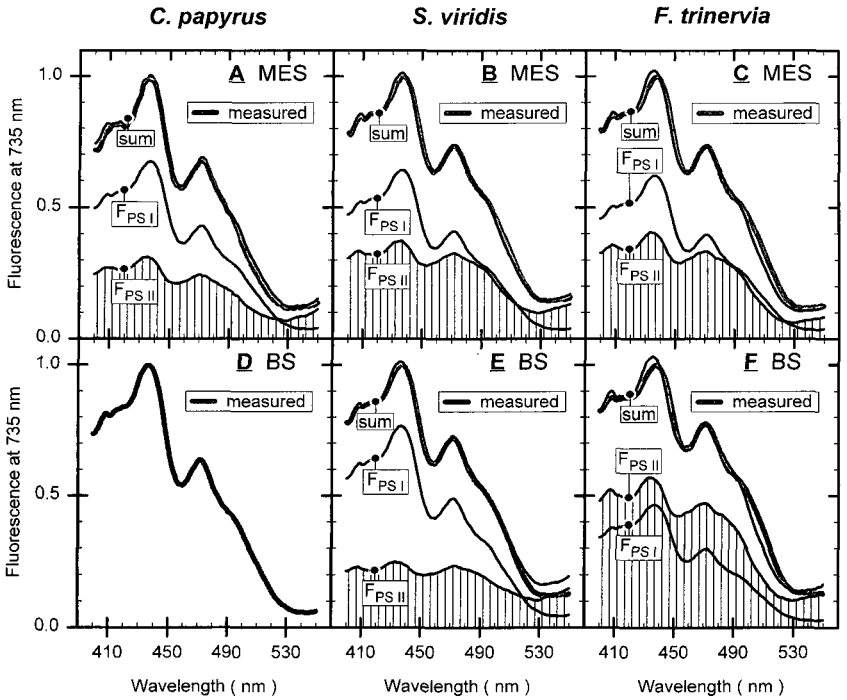

Figure 7. Deconvolution of excitation spectra of 735-nm fluorescence. Excitation spectra of 735-nm fluorescence are drawn with gray lines (taken from Fig. 4). Upper panels contain curves of mesophyll thylakoids (MES); spectra of bundle-sheath thylakoids are shown in the panels below (BS). Data derived from *C. papyrus* are depicted in A and D, of *S. viridis* in B and E, and of *F. trinervia* in C and F. Calculated spectra (black lines, labeled sum) resulted from varying PSI and PSII components until a best fit between the sum of both components and the measured curve was obtained. Curves labeled F_{PSI} and F_{PSII} (hatched area) are the PSI and PSII components, respectively, as determined by curve fitting. For curve fitting, the spectral range of 430 to 500 nm was considered. In all spectral simulations, the PSI curve used was the 77-K excitation spectrum of 735-nm fluorescence of bundle-sheath thylakoids of *C. papyrus* and corresponds to the average of seven measurements of two flow cytometric purifications. Because the PSI component and the experimental trace are similar, only the latter is shown in D. The PSII component was the 77-K excitation spectrum of 685-nm fluorescence of the thylakoid preparation to be analyzed.

relative values of Φ_T were lower in bundle-sheath thylakoids than in mesophyll thylakoids in all NAD-ME species except *A. spongiosa*.

DISCUSSION

Flow Cytometry of NADP-ME Species Compared with NAD-ME Species

By measuring Chl fluorescence at two spectral windows, we characterized mesophyll and bundle-sheath thylakoids isolated by conventional procedures using flow cytometry. In species with C_4 photosynthesis of the NADP-ME type, flow cytometric histograms revealed two-particle populations in both mesophyll and bundle-sheath thylakoids (Fig. 1, A–C). In earlier experiments with the NADP-ME species *Z. mays*, we unequivocally identified the population with high short-to-long-wavelength fluorescence ratio as mesophyll thylakoids; the peak at low fluorescence ratios corresponded to bundle-sheath thylakoids (Pfündel and Meister, 1996).

The fact that two peaks existed in conventionally prepared thylakoid fractions implies that our mesophyll and bundle-sheath preparations were significantly contaminated with other thylakoids (Fig. 1). This would be expected, since we did not attempt to optimize the purification procedure. Independent of the extent of cross-contamination, the conventionally prepared bundle-sheath thylakoids always contained a higher level of pure bundle-sheath thylakoids than did conventionally prepared mesophyll thylakoids.

Among all NADP-ME species, *C. papyrus* showed the smallest fraction of pure bundle-sheath thylakoids in conventionally prepared bundle-sheath thylakoids (Fig. 1A). Low yields of bundle-sheath thylakoids might indicate the presence of anatomical peculiarities that restrict access to bundle-sheath cells. In leaves of *Cyperus esculentus*, a layer of small cells without chloroplasts interposed between mesophyll and bundle-sheath cells has been described (Laetsch, 1971). The existence of such an additional cell layer in *C. papyrus* could explain the small population of pure bundle-sheath thylakoids.

Conventionally prepared thylakoid fractions of C_4 species with NAD-ME photosynthesis were also analyzed by flow cytometry. Like NADP-ME species, significant cross-contamination was apparent in the histograms (not shown). In contrast to NADP-ME species, bundle-sheath thylakoids always contained higher numbers of particles with high short-to-long-wavelength fluorescence ratios compared with mesophyll preparations.

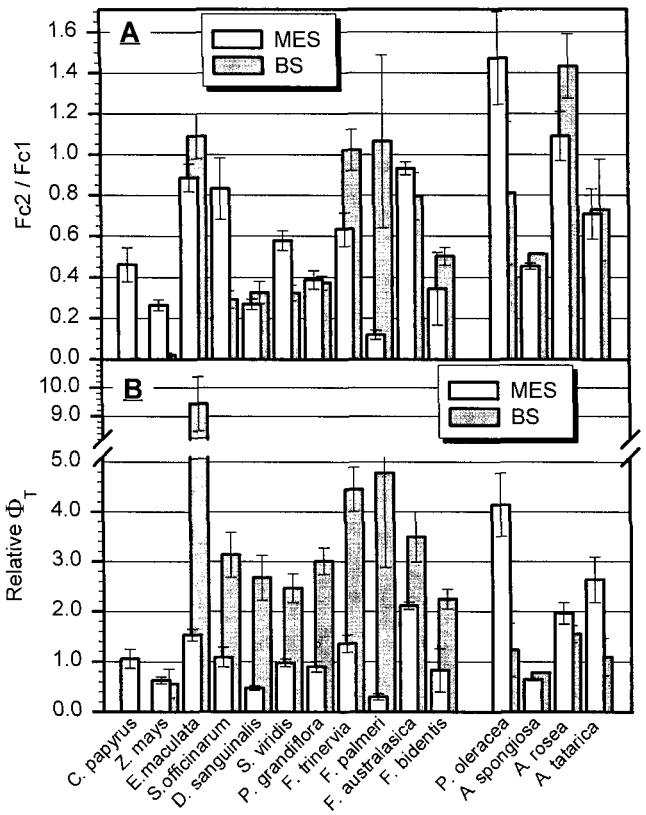

Figure 8. Contribution of PSII absorption to excitation spectra of 735-nm fluorescence and relative quantum yields of energy transfer. Results obtained with mesophyll (open bars) and bundle-sheath thylakoids (gray bars) purified by flow cytometry isolated from 15 different species are shown. Individual species are identified by abscissa labels in B. Data in A result from deconvolution of fluorescence excitation spectra as shown in Figure 7; the values correspond to the coefficient of the PSII spectral component (*Fc2*) relative to the PSI spectral component (*Fc1*). B shows quantum yields of energy transfer from PSII to PSI that were derived from parameters in A and PSII-to-PSI ratios as specified in "Appendix." Means of three to five determinations ± SD are given.

The differences between NADP-ME and NAD-ME species detected by flow cytometry are paralleled by published fluorescence data. In NADP-ME species, fluorescence emission spectroscopy revealed lower short-wavelength emission in bundle-sheath thylakoids than in mesophyll thylakoids; the inverse relation was established for NAD-ME species (Woo et al., 1970; Mayne et al., 1974). Thus, in NAD-ME species the fraction with the high fluorescence ratio, which is enriched using the conventional procedure for the isolation of bundle-sheath thylakoids, evidently corresponds to pure bundle-sheath thylakoids.

Flow Cytometrically Detected Fluorescence Characteristics and Fluorescence Emission Spectra

In the previous section, different fluorescence patterns for NADP-ME and NAD-ME types of C_4 photosynthesis were established by flow cytometry. Within the two biochemical types, varying differences between positions of the peaks of mesophyll thylakoids and bundle-sheath thylakoids were observed (Figs. 2). To characterize the individual thylakoid populations by fluorescence spectroscopy, pure mesophyll and bundle-sheath thylakoids were sorted by flow cytometry.

Generally, histogram peaks of pure mesophyll thylakoids were clearly separated from peaks of pure bundle-sheath thylakoids, and peak positions of pure thylakoids agreed with corresponding populations in histograms of conventionally isolated thylakoid preparations, as illustrated for three species in Figure 1. We infer from this that thylakoids purified with flow cytometry actually represent the populations observed in conventionally prepared thylakoids.

We also investigated the authenticity of pure thylakoids by comparing flow cytometry results of conventionally prepared thylakoids with low-temperature fluorescence emission of pure thylakoids. In pure mesophyll and bundle-sheath thylakoids, the short-to-long-wavelength fluorescence ratio was derived from low-temperature emission spectra. These fluorescence ratios were linearly related to the peak positions in frequency diagrams when data from mesophyll thylakoids were expressed relative to the values for bundle-sheath thylakoids (Fig. 2B). In essence, linearity between the two parameters establishes that thylakoids purified by flow cytometry actually represent the populations in conventionally prepared thylakoid preparations.

Relation between Fluorescence Emission and Chl *a/b* Ratios

Ratios of short-to-long-wavelength fluorescence derived from emission spectra of pure thylakoid fractions varied considerably among species, and between mesophyll and bundle-sheath thylakoids of individual species (Fig. 2A). At low temperatures, Chl fluorescence at wavelengths below 700 nm is attributed to PSII; most Chl fluorescence at wavelengths above 700 nm is emitted by PSI (Govindjee, 1995). Therefore, we presume that varying ratios of short-to-long-wavelength fluorescence indicate varying PSII-to-PSI ratios.

To test our hypothesis, we compared short-to-long-wavelength fluorescence ratios with PSII-to-PSI ratios derived from Chl *a/b* values, as specified in "Appendix." Photosystem ratios of all samples were proportional to corresponding short-to-long-wavelength fluorescence of emission spectra (Fig. 3B). The linear relationship indicates that short-to-long-wavelength fluorescence ratios are indeed related to the photosystem ratios in thylakoids.

Consequently, the marked short-wavelength emission observed in bundle-sheath thylakoids of many NADP-ME species (Figs. 1, H and I, and 2A) demonstrates significant amounts of PSII in those thylakoids. A discussion of possible reasons that our PSII-to-PSI ratios were lower than the ratios of PSII-to-PSI reaction centers published earlier is presented in "Appendix."

For all NADP-ME species, our calculations yielded higher PSII-to-PSI ratios in mesophyll thylakoids than in bundle-sheath thylakoids (Fig. 3B). All of the NAD-ME species exhibited the inverse relation, with the exception of

A. spongiosa. The ratio of ATP/NADPH required for CO_2 fixation is lower in mesophyll cells than in bundle-sheath cells in NADP-ME species (Hatch, 1987); the opposite is true for NAD-ME species. NADP reduction depends on linear electron transport through PSII and PSI. ATP formation can potentially be driven by cyclic electron transport around PSI. Hence, when high ATP/NADPH ratios are required for CO_2 fixation, low PSII-to-PSI ratios are expected. Therefore, we conclude that our photosystem ratios agree with the current perception of C_4 photosynthesis.

Energy Transfer between Photosystems

Excitation spectra of Chl fluorescence at 685 and 735 nm were recorded from pure mesophyll thylakoids and bundle-sheath thylakoids from all species. The size of the 475-nm maximum relative to the maximum at 435 nm was used to classify the spectra (Fig. 5).

Generally, excitation spectra of 685-nm fluorescence showed higher 475-nm bands than 735-nm excitation spectra (Fig. 5). This is to be expected, since 685-nm emission can be attributed to PSII (Govindjee, 1995), and the PSII holo-complex is enriched in Chl *b* that absorbs in vivo at about 475 nm (Siefermann-Harms and Ninnemann, 1982). An exception to this general trend are bundle-sheath thylakoids of *E. maculata*; at present, we cannot explain the distinctive spectral properties of these thylakoids.

We investigated whether a relationship exists between the 475-nm values of excitation spectra and the relative fluorescence at 685 nm in emission spectra. Linear correlation between the two parameters was observed in bundle-sheath thylakoids from NADP-ME species (Fig. 6). An exception to this trend was *E. maculata*.

As discussed above, the short-to-long-wavelength emission ratios are correlated with PSII-to-PSI ratios. This means that the size of the 475-nm maximum is related to the abundance of PSII in bundle-sheath thylakoids from NADP-ME species. Because the relative absorption at 475 nm of PSII is higher than that of PSI, it is reasonable to assume that PSII absorption accounts for the correlation between 475-nm excitation and fluorescence ratio.

The actual contribution of PSII to the functional light-harvesting antenna of PSI is not evident from excitation spectra. Hence, we chose spectral simulation as described in the Appendix to visualize the significance of PSII absorption. Since PSII fluorescence emission was virtually absent in pure bundle-sheath thylakoids from *C. papyrus* (Fig. 1G), we utilized the 735-nm excitation spectrum of these thylakoids as a model curve for PSI excitation. The excitation spectra at the 685-nm emission wavelength were used as PSII model curves because PSI emission is negligible at this wavelength.

Good correspondence between calculated and experimental spectra was obtained (Fig. 7). In some species, minor deviations between calculated and measured curves occurred in the range from 490 to 530 nm (compare Fig. 7, C and F). In this spectral region carotenoid absorption is expected (Pfündel and Baake, 1990). Because the same PSI model spectrum was used for all simulations, differences in carotenoid absorption between the model spectrum and the excitation spectrum of pure PSI of individual samples probably caused the discrepancy between experimental and simulated curves.

For bundle-sheath thylakoids of *F. trinervia*, spectral simulation indicates that the PSII component in the apparent PSI excitation spectrum was higher than that of PSI (Fig. 7F). A similar situation was found in bundle-sheath thylakoids of *E. maculata*, *F. australasica*, and *F. palmeri*, as demonstrated by comparable values of *Fc*2/*Fc*1 in Figure 8A. In most other bundle-sheath thylakoids from NADP-ME species, the PSII absorption that contributes to the total PSI excitation spectrum was smaller but remained significant (Figs. 7E and 8A). We conclude that in many bundle-sheath thylakoids of NADP-ME species, PSII absorption plays an important role in excitation spectra of 735-nm fluorescence.

PSII exhibits minor emission at its vibrational satellite band in the region of 735 nm (Govindjee, 1995). Thus, one explanation for the parallel increase of the 475-nm excitation peak and of the short-to-long-wavelength fluorescence emission ratios (Fig. 6) could be PSII fluorescence at 735 nm. If this is true, than the values for 475-nm excitation should generally parallel the PSII-to-PSI ratios.

In *F. trinervia*, fluorescence emission spectra indicated higher PSII-to-PSI ratios in mesophyll thylakoids than in bundle-sheath thylakoids (Fig. 1I). The estimated PSII component in excitation spectra for 735 nm, however, was lower in mesophyll than in bundle-sheath thylakoids (Fig. 7, C and F). Comparable observations were made in most of NADP-ME species (compare Fig. 2 and Fig. 8). We conclude that PSII emission at 735 nm cannot account for the contribution of the PSII spectral component to the 735-nm excitation spectra. Thus, an energy transfer from PSII to PSI (compare Butler, 1978) must explain the linearity between the 475-nm values of PSI excitation spectra and the short-to-long-wavelength emission ratio (Fig. 6).

By assuming PSII-to-PSI energy transfer, relative numbers for the quantum yield of energy transfer from PSII to PSI were calculated as described in "Appendix." Experimental parameters entering the model were the quotient of *Fc*2/*Fc*1 and photosystem ratios as derived from Chl *a*/*b* values.

Our model calculations revealed a general pattern for species with NADP-ME photosynthesis: relative numbers of energy transfer yield were markedly higher in bundle-sheath thylakoids than in mesophyll thylakoids, with the exception of *C. papyrus* and *Z. mays*. Low yields of energy transfer in the latter two species are likely related to extremely low 685-nm fluorescence emission (Figs. 1G and 2A), which causes inaccurate excitation spectra of 685-nm fluorescence. Since the 685-nm excitation spectra were used to determine the PSII component in the 735-nm excitation spectra, the results of spectral simulations are probably unreliable in these two cases.

Differences in quantum yields observed for NADP-ME species agree with known chloroplast ultrastructure and physical characteristics of the two photosystems. In NADP-ME species, grana stacks are present in mesophyll chloroplasts and are depleted or absent in bundle-sheath

chloroplasts (Hatch, 1987). Also, in the genus *Flaveria* bundle-sheath chloroplasts are agranal (Keefe and Mets, 1983; Höfer et al., 1992), despite their relatively high concentrations of the PSII holo-complex (Fig. 3B; compare "Appendix"), which could have favored grana formation (Allen, 1992).

In granal chloroplasts most PSII is located in grana stacks and, hence, physically separated from PSI (Anderson, 1986). In agranal chloroplasts, the structural basis for separation of the photosystems is missing. When photosystems are in close contact, efficient energy transfer from PSII to PSI takes place because of the red-shifted absorption properties of PSI (Staehelin and Arntzen, 1983; Trissl and Wilhelm, 1993). In summary, we explain high yields of energy transfer in bundle-sheath thylakoids of NADP-ME species by a relatively even distribution of photosystems.

In contrast to NADP-ME species, most plants with NAD-ME photosynthesis exhibited lower yields of energy transfer in bundle-sheath thylakoids than in mesophyll thylakoids (Fig. 8B). In NAD-ME species grana are present in mesophyll and bundle-sheath chloroplasts (Hattersley and Watson, 1992). With the above considerations one would expect a higher degree of grana formation in bundle-sheath thylakoids. This has actually been shown in NAD-ME species of the genus *Atriplex* (Pyliotis et al., 1971; Liu and Dengler, 1994). Thus, the correspondence between relative yields of energy transfer and chloroplast ultrastructure in plants with NADP-ME or NAD-ME photosynthesis stresses the validity of our model calculations.

Function of PSII in NADP-ME Bundle-Sheath Thylakoids

At variance to most of the conclusions drawn from activity measurements of PSII (Edwards and Walker, 1983; Hatch, 1987), we have clearly demonstrated the presence of significant amounts of PSII in bundle-sheath thylakoids in many of our NADP-ME species. Except for *C. papyrus* and *Z. mays*, the relative yield of energy transfer to PSI (relative Φ_T) was considerably higher in bundle-sheath thylakoids than in mesophyll thylakoids in all NADP-ME species (Fig. 8B).

Without *C. papyrus* and *Z. mays*, the average increase in the yield was 3.7-fold. We are aware that the value of 3.7 is only a crude approximation and is affected by some uncertain estimates of quantum yields. Examples are the extremely high relative Φ_T in pure bundle-sheath thylakoids from *E. maculata* and the very low relative Φ_T in pure mesophyll thylakoids of *F. palmeri* (Fig. 8A).

The high yields of energy transfer in bundle-sheath chloroplasts from NADP-ME species were derived from measurements at 77 K, i.e. under conditions that arrest photochemical reactions. Efficient energy transfer probably also exists at room temperature in vivo, because recent reports suggest the presence of inactive PSII reaction centers in bundle-sheath chloroplasts of NADP-ME species (Höfer et al., 1992; Meierhoff and Westhoff, 1993; Bassi et al., 1995). In essence, we suggest that PSII acts primarily as an antenna for PSI in bundle-sheath thylakoids of many species with NADP-ME photosynthesis.

Our model calculations address predominantly PSII complexes in which the Chl *a*/*b*-binding LHCII makes up the bulk of the antenna (discussed in "Appendix"). Hence, our conclusions agree with those of Bassi and co-workers (Bassi and Simpson, 1986; Bassi et al., 1995), who indicated that LHCII functions as an antenna to PSI in bundle-sheath chloroplasts of *Z. mays*. The fact that our Chl *a*/*b* ratios do not indicate significant amounts of light-harvesting complex in bundle-sheath thylakoids of *Z. mays* (Fig. 3A) is probably related to different developmental stages (compare Dai et al., 1995) of the plants used.

Due to the high Chl *b* content of LHCII, the functional association of PSII and PSI in bundle-sheath chloroplasts of NADP-ME species reduces the absorption gap of PSI in the green spectral region. We suggest that the extended spectral range of PSI absorption is important for efficient light-harvesting of PSI in the bundle sheath. To assess the significance of PSII absorption in the bundle sheath of NADP-ME species in vivo, detailed information on the light gradients in leaves of C_4 species is necessary. Most studies on light gradients in green leaves were carried out with C_3 species (compare Vogelmann, 1993). Since the leaf anatomy of C_3 and C_4 plants differs markedly, these results cannot be directly applied to C_4 species. Furthermore, because the light climate in leaves of C_4 plants has not been studied extensively, it is difficult to speculate why significant levels of PSII have not been detected in our bundle-sheath thylakoids of *Z. mays* and *C. papyrus*.

It has been proposed that LHCII plays a key role in dissipation of excess excitation energy (Horton et al., 1991); in the current study it contributed significantly to the antenna of bundle-sheath PSI in many NADP-ME species. Studies carried out mostly with C_3 plants suggest that the violaxanthin cycle regulates energy dissipation in response to environmental stress (reviewed by Pfündel and Bilger, 1994). The functional violaxanthin cycle has been demonstrated in bundle-sheath chloroplasts of the C_4 species *Z. mays* (Thayer and Björkman, 1992). Consequently, the regulation of energy dissipation as postulated above may occur in a similar way in the bundle-sheath chloroplasts of NADP-ME species.

APPENDIX

Our data indicated that energy transfer between PSII and PSI occurs (see "Discussion"). To explain this in more detail, we wanted to estimate the ratios of the photosystems involved and the quantum yield of energy transfer from PSII to PSI. Flow cytometry yields dilute thylakoid suspensions that are sufficient for steady-state Chl fluorescence analysis, but not concentrated enough to apply the classical methods for determinations of photosystem stoichiometries (compare Melis, 1989) or of PSII-to-PSI energy transfer (compare Butler, 1978). Hence, we derived equations to estimate these parameters from steady-state fluorescence measurements.

PSII-to-PSI Ratio

Photosystem stoichiometries were derived from Chl *a*/*b* ratios. In the most simple case, two homogeneous pools of photosystems have to be considered: PSI and PSII. Hence, the concentration of Chl *a* (c_{Chla}) is the sum of the concen-

tration of PSI (c_{PS1}) times the number of molecules of Chl *a* in PSI ($N_{Chla,PS1}$) plus the concentration of PSII (c_{PS2}) times the number of molecules of Chl *a* in PSII ($N_{Chla,PS2}$):

$$c_{Chla} = c_{PS1} \times N_{Chla,PS1} + c_{PS2} \times N_{Chla,PS2} \quad (1)$$

Equivalently, the concentration of Chl *b* (c_{Chlb}) is given by:

$$c_{Chlb} = c_{PS1} \times N_{Chlb,PS1} + c_{PS2} \times N_{Chlb,PS2} \quad (2)$$

where $N_{Chlb,PS1}$ and $N_{Chlb,PS2}$ are the numbers of molecules of Chl *b* in PSI and PSII, respectively. Combination of Equations 1 and 2 yields the ratio of PSII to PSI as a function of the Chl *a*/*b* ratio of a sample:

$$\frac{c_{PS2}}{c_{PS1}} = \frac{N_{Chlb,PS1}}{N_{Chlb,PS2}} \times \frac{(N_{Chla,PS1}/N_{Chlb,PS1} - c_{Chla}/c_{Chlb})}{(c_{Chla}/c_{Chlb} - N_{Chla,PS2}/N_{Chlb,PS2})} \quad (3)$$

Estimation of PSII-to-PSI Ratios in Vivo

Equation 3 is valid only if the two photosystems in our samples can be treated as homogeneous pools, and if the pigment stoichiometry of PSI and PSII is similar for different samples.

In the case of PSI, we assume one homogeneous population in our samples. The heterogeneity in PSI antenna size, as reported by Andreasson and Albertsson (1993), does not need to be considered here because it was attributed to a functional connection between LHCII and PSI and will be treated as a PSII-to-PSI energy transfer in our model.

We assumed that all PSI subcomplexes were similar in the species studied because the PSI core antenna is conserved among cyanobacteria, green algae, and higher plants (Golbeck, 1992), and high sequence homology exists between LHCI polypeptides from different higher-plant species (Jansson, 1994).

PSI appears to be present in its mature form in all of our samples because we always observed a distinct fluorescence band located between 730 and 735 nm. The long-wavelength fluorescence was attributed to the peripheral LHCI-730 complex (Mukerji and Sauer, 1990; Tjus et al., 1995) and indicates that complete assembly of the PSI holo-complex had occurred (Schuster et al., 1985; Anandan et al., 1993; Dreyfuss and Thornber, 1994).

The antenna size of the mature PSI complex is assumed to be largely insensitive to possible differences in the light characteristics between the mesophyll and bundle-sheath compartment. We infer this from the relatively constant levels of the PSI antenna under growth conditions that caused significant alterations in the PSII antenna size (Leong and Anderson, 1984; Humbeck et al., 1994). Furthermore, for the PSI complex, similar carotenoid and Chl compositions were reported for cotton, a C_3 plant, and for bundle-sheath thylakoids from maize (Thayer and Björkman, 1992). The same subunit composition, matching absorbance, and 77-K fluorescence emission spectra were found in mesophyll and bundle-sheath chloroplasts of maize (Bassi 1985).

In contrast to PSI at least two PSII groups exist that differ in their antenna size (Melis, 1991): $PSII_\alpha$ with about 250 molecules Chl *a*+*b* and $PSII_\beta$, in which the number of Chl *a*+*b* is reduced by about 50%. $PSII_\beta$ occurs at about 33% of the concentration of $PSII_\alpha$. The Chl *a*/*b* ratios were 1.6 and 2.8 to approximately 6 in $PSII_\alpha$ and $PSII_\beta$, respectively (Melis et al., 1987; Melis, 1989).

In our model, we are concerned with the transfer of light energy absorbed by PSII to PSI. Consequently, the concentration of PSII complexes with high absorption, i.e. $PSII_\alpha$, is especially important for our considerations. PSII reaction centers with small antenna sizes, i.e. $PSII_\beta$, play only a minor role in steady-state fluorescence measurements. In fact, in the wavelength range of our excitation spectra, the light-harvesting efficiency of $PSII_\beta$ relative to $PSII_\alpha$ is even less than is suggested by their Chl *a*+*b* contents as substantiated below:

(a) In the spectral region from 400 to 550 nm, Chl *b* is more effective in light absorption than Chl *a*, as judged from the absorption coefficients of the respective Soret bands in vitro (compare Lichtenthaler, 1987). Chl *a*/*b* values indicate that the relative contribution of Chl *b* to light absorption in $PSII_\beta$ is less than that of $PSII_\alpha$. Hence, $PSII_\beta$ is expected to show decreased Chl absorption when one normalizes it in terms of moles of Chl *a*+*b*.

(b) The increased Chl *a*/*b* ratios in $PSII_\beta$ (see above) indicate decreased amounts of the Chl *a*/*b*-binding-LHCII. Similar stoichiometric ratios of carotenoid to Chl are present in the PSII core complex and in LHCII (Alfonso et al., 1994; Ruban et al., 1994). Xanthophylls contribute significantly to the absorbance of LHCII in the spectral region from 390 to 530 nm and energy transfer from carotenoid to Chl occurs with virtually 100% efficiency (Siefermann-Harms, 1987). In comparison, the carotenoid-to-Chl energy transfer of β-carotene, the main carotenoid of the PSII core complex, occurs with lower efficiencies (Hashimoto and Koyama, 1990; Alfonso et al., 1994). Thus, decreased amounts of LHCII in $PSII_\beta$ implies decreased light harvesting by carotenoids when normalized to moles of Chl *a*+*b*.

Because of its small functional antenna, we neglect $PSII_\beta$ and estimated PSII-to-PSI ratios from the Chl content of $PSII_\alpha$ as summarized by Melis (1991). The approximated numbers for $PSII_\alpha$ used were 150 Chl *a* molecules ($N_{Chla,PS2}$) and 100 Chl *b* molecules ($N_{Chlb,PS2}$). For PSI, the Chl *a* content ($N_{Chla,PS1}$) was set to 180, and 20 molecules of Chl *b* ($N_{Chlb,PS1}$) were presumed (Melis, 1991). Introducing these pigment stoichiometries into Equation 3 yields:

$$\frac{c_{PS2}}{c_{PS1}} = \frac{1}{5} \times \frac{(9 - c_{Chla}/c_{Chlb})}{(c_{Chla}/c_{Chlb} - 3/2)} \quad (4)$$

Equation 4 was derived using the approximate pigment stoichiometries of $PSII_\alpha$. $PSII_\beta$ has only a minor influence on Equation 4 according to the simple model calculations presented below. We computed Chl *a*/*b* values by assuming the presence or absence of $PSII_\beta$. For our calculations, we used a constant PSI concentration that was arbitrarily set to 1, a $PSII_\alpha$ concentration that ranged between 0.025 and 1, and a $PSII_\beta$ concentration that was always 33% of $PSII_\alpha$.

By applying the pigment stoichiometries of Equation 4 for PSI and $PSII_\alpha$, and assuming 85 Chl *a* and 30 Chl *b* for $PSII_\beta$ (Melis, 1989), we obtained Chl *a*/*b* values that matched our experimental data. For the two series of Chl *a*/*b* values, photosystem ratios were derived from Equation 4. Generally, the presence of $PSII_\beta$ resulted in a slight overestimation of PSII-to-PSI ratios. The maximum deviation was 7.7%. We repeated our calculation under the assumption that $PSII_\beta$ lacks LHCII and assumed that only 50 molecules of Chl *a* were present in $PSII_\beta$. In this case, we underestimated the PSII-to-PSI ratios by at most 12%.

The insensitivity of our photosystem ratios toward $PSII_\beta$ could explain why even our highest PSII-to-PSI ratios were lower than published ratios. The published values were derived from reaction-center-dependent signals and were, therefore, largely independent of the PSII antenna size (Graan and Ort, 1984; Wild et al., 1986; Ghirardi and Melis, 1988; Melis, 1989; Walters and Horton, 1994).

Depending on growth conditions, the antenna size of $PSII_\alpha$ may vary (Anderson et al., 1995). We used similar growth conditions for all of the species. However, different $PSII_\alpha$ antenna sizes could have been triggered by different light climates in mesophyll and bundle-sheath compartments.

In analogy to our calculations for $PSII_\beta$, we assessed the effect of a varying $PSII_\alpha$ antenna size on photosystem ratios. By assuming that the numbers of Chl *a*+*b* in $PSII_\alpha$ are reduced by about 33%, i.e. by 40 Chl *a* molecules and 40 Chl *b* molecules, we found that the photosystem ratios obtained with Equation 4 were decreased by 43 to 49%. Hence, variations in the $PSII_\alpha$ antenna size could influence our photosystem estimates.

However, for NADP-ME and NAD-ME species we obtained significantly different mesophyll/bundle-sheath patterns of photosystem ratios. Our results agree with the specific NADPH and ATP requirements for CO_2 fixation of the two groups of C_4 species (see "Discussion"), indicating that within a C_4 leaf variations in the $PSII_\alpha$ antenna size is not the dominating factor. Furthermore, among different species our photosystem ratios appear reasonable because we generally observed that the samples with the lowest PSII-to-PSI ratios exhibit the lowest ratios of PSII-to-PSI fluorescence emission and vice versa (Fig. 3B).

We cannot exclude that particular species-dependent differences lead to erroneous photosystem estimates for individual plants. For example, the mesophyll thylakoids from *S. officinarum* exhibited a significantly higher PSII-to-PSI ratio compared with those of all other mesophyll thylakoids from NADP-ME species (Fig. 3).

In summary, our estimates of PSII-to-PSI ratios address mainly the PSII complexes with large antennae and are appropriate when steady-state fluorescence spectra are considered. Reliable conclusions can be drawn when the results from a large number of species are compared, as is the case in the present study.

Quantum Yields of Energy Transfer

Energy transfer from PSII to PSI was estimated by a model that utilizes as input empirical fluorescence excitation spectra. The excitation spectra were recorded at 77 K, with 685 or 735 nm as the emission wavelength. At 77 K, fluorescence at 685 nm originates from PSII, and fluorescence at 735 nm is dominated by PSI but also contains some PSII emission (Govindjee, 1995), which is not considered in our calculations.

In our model, screening and fluorescence reabsorption artifacts are disregarded because we are dealing with extremely diluted samples. Quantum flux density in excitation spectra is treated as constant since wavelength-dependent intensity changes of the excitation source are corrected by the fluorimeter.

As we did with the determination of photosystem ratios, we assume two components in our fluorescence excitation spectra: PSI and PSII. Because we also assume the existence of PSII to PSI energy transfer (see "Discussion"), the light absorption by PSI and PSII should contribute to PSI excitation spectra in situ.

In the case of PSI, absorption and excitation spectra differ: the Chl *a* that emits at 735 nm is situated in the Chl *b*-enriched LHCI and is preferably excited by the Chl *b* nearby (Mukerji and Sauer, 1990; Tjus et al., 1995). This can be explained by slowed-down energy transfer times at low temperatures (Holzwarth, 1991; Wittmershaus et al., 1992), which prevent rapid delocalization of the excited state. Because of competing decay pathways for excited states, the position of the light-absorbing pigment relative to the position of the fluorophore influences the probability that an excited state is trapped by the low-energy Chl *a*.

With the above considerations, one can formulate for the fluorescence of pure PSI excited at wavelength λex as follows:

$$F_{735}^{PS1}(\lambda ex) = \Phi_{F735} \times L_{PS1}^{A}(\lambda ex) \times A_{PS1}(\lambda ex) \quad (5)$$

where $A_{PS1}(\lambda ex)$ is the absorption of PSI at λex, and $L_{PS1}^{A}(\lambda ex)$ is a wavelength-dependent correction factor that considers the fact that the absorption properties of the pigments close to the fluorescing Chl *a* differ from that of the PSI holo-complex, and Φ_{F735} is the fluorescence yield of the fluorophore.

In excited states originating from the PSII-to-PSI energy transfer, the distance between the position at which excitation occurs and the fluorophore influences the probability that an excited state is trapped by the fluorescing Chl *a*. PSII-to-PSI energy transfer involves excited Chl states, which have energies corresponding to the red spectral region (Govindjee, 1995). Here, we deal with excitation spectra in the range between 400 and 550 nm. Consequently, for PSII-to-PSI energy transfer, we consider the spatial dependence that an excited state is trapped by the fluorescing Chl *a* by introducing a wavelength-independent correction factor. Hence, the fluorescence of PSI in situ is described by:

$$F_{735}(\lambda ex) = \Phi_{F735} \times (L_{PS1}^{A}[\lambda ex] \times A_{PS1}[\lambda ex] + L_{PS1}^{T} \times \Phi_T \times A_{PS2}[\lambda ex]) \quad (6)$$

where $A_{PS2}(\lambda ex)$ denotes the PSII absorption at λex, and Φ_T is the quantum yield of PSII-to-PSI energy transfer.

Replacing in Equation 6 the parameter A_{PS1} (λex) by the spectrum of PSI absorption coefficients, α_{PS1}(λex), times PSI concentration, c_{PS1}, and A_{PS2} (λex) by α_{PS2} (λex) times c_{PS2} yields:

$$F_{735}(\lambda ex) = \Phi_{F735} \times (L_{PS1}{}^{A}(\lambda ex) \times \alpha_{PS1}(\lambda ex) \times c_{PS1} + L_{PS1}{}^{T} \times \Phi_T \cdot \alpha_{PS2}(\lambda ex) \times c_{PS2}) \quad (7)$$

The spectrum of absorption coefficients of PSI can be related to the excitation spectrum of pure PSI according to:

$$\alpha_{PS1}(\lambda ex) = \frac{N1 \times e_{PS1}(\lambda ex)}{\Phi_{F735} \times L_{PS1}{}^{A}(\lambda ex)} \quad (8)$$

where $N1$ is a proportionality factor that depends on the fluorimeter sensitivity at 735 nm.

In the case of PSII, we assume that absorption spectra are proportional to excitation spectra for the following reason: the size of the Chl *b* band (475nm) relative to the main excitation peak was ≥0.75 in our excitation spectra (Fig. 5). In comparison, values close to 0.75 were reported for the absorbance spectrum from isolated LHCII, which constitutes the bulk of the PSII antenna (Bassi and Dainese, 1992; Hemelrijk et al., 1992). If, as in PSI, the fluorescing Chl *a* primarily reflects the absorption properties of the pigments nearby, then the relative Chl *b* band contributing to excitation spectra is expected to be markedly lower than the corresponding value in absorbance spectra. This is because at 77 K, most of the PSII fluorescence originates from Chl *a* in the PSII core antenna (Rijgersberg et al., 1979), and the PSII core antenna lacks Chl *b* (Peter and Thornber, 1991). Hence, one can formulate:

$$\alpha_{PS2}(\lambda ex) = e_{PS2}(\lambda ex) \times N2 \quad (9)$$

where $N2$ takes into account the fluorimeter sensitivity at 685 nm emission wavelength. Replacing in Equation 7 the spectra of absorbance coefficient with Equation 8 and Equation 9 yields:

$$F_{735}(\lambda ex) = N1 \times c_{PS1} \times e_{PS1}(\lambda ex) + \Phi_{F735} \times L_{PS1}{}^{T} \times \Phi_T \times N2 \times c_{PS2} \times e_{PS2}(\lambda ex) \quad (10)$$

We deconvoluted our excitation spectra for 735-nm fluorescence according to:

$$F_{735}(\lambda ex) = Fc1 \times e_{PS1}(\lambda ex) + Fc2 \times e_{PS2}(\lambda ex) \quad (11)$$

Here, e_{PS1}(λex) and e_{PS2}(λex) are fluorescence excitation spectra of pure PSI and PSII, and $Fc1$ and $Fc2$ are free parameters. As e_{PS1}(λex), the excitation spectrum of pure bundle-sheath thylakoids from *C. papyrus* was used. This spectrum was chosen because virtually no PSII emission was apparent in bundle-sheath thylakoids from *C. papyrus*. Because of the arguments summarized above (see "Estimation of PSII-to-PSI Ratios in Vivo"), we assume that the excitation spectra of PSI are comparable in all of our samples. As e_{PS2}(λex), the excitation spectra of 685-nm fluorescence of the individual samples were used. All excitation spectra were normalized to their maximum at 435 nm.

Equation 11 is similar to Equation 10. The comparison of coefficients yields:

$$Fc1 = N1 \times c_{PS1} \quad (12a)$$

and

$$Fc2 = \Phi_{F735} \times L_{PS1}{}^{T} \times \Phi_T \times N2 \times c_{PS2} \quad (12b)$$

Division of Equation 12b by Equation 12a results in:

$$\Phi_T \times \Phi_{F735} \times L_{PS1}{}^{T} \times \frac{N2}{N1} = \frac{Fc2}{Fc1} \times \frac{c_{PS1}}{c_{PS2}} \quad (13)$$

In Equation 13, the factors $N1$ and $N2$ are dependent on the fluorimeter used and can be assumed to be a constant for different measurements. As explained above, we expect similar behavior by PSI in the different thylakoid fractions investigated and, therefore, Φ_{F735} and $L_{PS1}{}^{T}$ are assumed to be comparable for the different samples. Consequently, Equation 13 permits us to estimate relative quantum yields for PSII-to-PSI energy transfer from the factors $Fc1$ and $Fc2$ obtained from Equation 6 and from PSI-to-PSII ratios as derived from Equation 4.

ACKNOWLEDGMENT

For critically reading the manuscript we thank Dr. David Waddell.

Received March 13, 1996; accepted July 26, 1996.

LITERATURE CITED

Alfonso M, Montoya G, Cases R, Rodríguez R, Picorel R (1994) Core antenna complexes, CP43 and CP47, of higher plant photosystem II. Spectral properties, pigment stoichiometry, and amino acid composition. Biochemistry **33:** 10494–10500

Allen JF (1992) How does protein phosphorylation regulate photosynthesis. Trends Biochem Sci **17:** 12–17

Anandan S, Morishige DT, Thornber JP (1993) Light-induced biogenesis of light-harvesting complex I (LHC I) during chloroplast development in barley (*Hordeum vulgare*). Studies using the cDNA clones of the 21- and 20-kilodalton LHC I apoproteins. Plant Physiol **101:** 227–236

Anderson JM (1986) Photoregulation of the composition, function, and structure of thylakoid membranes. Annu Rev Plant Physiol **37:** 93–136

Anderson JM, Chow WS, Park Y-I (1995) The grand design of photosynthesis: acclimation of the photosynthetic apparatus to environmental cues. Photosynth Res **46:** 129–139

Andreasson E, Albertsson P-Å (1993) Heterogeneity in photosystem I: the larger antenna of photosystem Iα is due to functional connection to a special pool of LHCII. Biochim Biophys Acta: **1141:** 175–182

Bassi R (1985) Spectral properties and polypeptide composition of the chlorophyll-proteins from thylakoids of granal and agranal chloroplasts of maize (*Z. mays* L.). Carlsberg Res Commun **50:** 127–143

Bassi R, Dainese P (1992) A supramolecular light-harvesting complex from chloroplast photosystem-II membranes. Eur J Biochem **204:** 317–326

Bassi R, Marquardt J, Lavergne J (1995) Biochemical and functional properties of photosystem II in agranal membranes from

maize mesophyll and bundle sheath chloroplasts. Eur J Biochem **233:** 709–719

Bassi R, Simpson DJ (1986) Differential expression of LHCII genes in mesophyll and bundle sheath cells of maize. Carlsberg Res Commun **51:** 363–370

Brown WV (1977) The Kranz syndrome and its subtypes in grass systematics. Mem Torrey Bot Club **23:** 1–97

Bruhl JJ, Stone NE, Hattersley PW (1987) C_4 acid decarboxylation enzymes and anatomy in sedges (Cyperaceae): first record of NAD-malic enzyme species. Aust J Plant Physiol **14:** 719–728

Butler WL (1978) Energy distribution in the photochemical apparatus of photosynthesis. Annu Rev Plant Physiol **29:** 345–378

Dai Z, Ku MSB, Edwards GE (1995) C_4 photosynthesis. The effects of leaf development on the CO_2-concentrating mechanism and photorespiration in maize. Plant Physiol **107:** 815–825

Dreyfuss BW, Thornber JP (1994) Organization of the light-harvesting complex of photosystem I and its assembly during plastid development. Plant Physiol **106:** 841–848

Edwards G, Walker D (1983) C_3, C_4: Mechanisms, and Cellular and Environmental Regulation, of Photosynthesis. Blackwell Scientific, Oxford, UK

Ghirardi ML, Melis A (1988) Chl *b* deficiency in soybean mutants. I. Effects on photosystem stoichiometry and chlorophyll antennae size. Biochim Biophys Acta **932:** 130–137

Golbeck JH (1992) Structure and function of photosystem I. Annu Rev Plant Physiol Plant Mol Biol **43:** 293–324

Govindjee (1995) Sixty-three years since Kautsky: chlorophyll *a* fluorescence. Aust J Plant Physiol **22:** 131–160

Graan T, Ort DR (1984) Quantitation of the rapid electron donors to P_{700}, the functional plastoquinone pool, and the ratio of the photosystems in spinach chloroplasts. J Biol Chem **259:** 14003–14010

Hashimoto H, Koyama Y (1990) The 2^1A_g state of a carotenoid bound to spinach chloroplasts as revealed by picosecond transient Raman spectroscopy. Biochim Biophys Acta **1017:** 181–186

Hatch MD (1987) C_4 photosynthesis: a unique blend of modified biochemistry, anatomy and ultrastructure. Biochim Biophys Acta **895:** 81–106

Hatch MD (1992) C_4 photosynthesis: an unlike process full of surprises. Plant Cell Physiol **33:** 333–342

Hattersley PW, Watson L (1992) Diversification of photosynthesis. *In* GP Chapman, ed, Grass Evolution and Domestication. Cambridge University Press, Cambridge, UK, pp 38–116

Heber U, Schmitt JM, Krause GH, Klosson RJ, Santarius KA (1981) Freezing damage to thylakoid membranes *in vitro* and *in vivo*. *In* GJ Morris, A Clarke, eds, Effects of Low Temperatures on Biological Membranes. Academic Press, Cambridge, UK, pp 263–288

Hemelrijk PW, Kwa SLS, van Grondelle R, Dekker JP (1992) Spectroscopic properties of LHC-II, the main light-harvesting chlorophyll a/b protein complex from chloroplasts membranes. Biochim Biophys Acta **1098:** 159–166

Höfer MU, Santore UJ, Westhoff P (1992) Differential accumulation of the 10-, 16- and 23-kDa peripheral components of the water-splitting complex of photosystem II in mesophyll and bundle-sheath chloroplasts of the dicotyledonous C_4 plant *Flaveria trinervia* (Spreng.) C. Mohr. Planta **186:** 304–312

Holzwarth AR (1991) Excited-state kinetics in chlorophyll systems and its relationship to the functional organization of the photosystems. *In* H Scheer, ed, Chlorophylls. CRC Press, Boca Raton, FL, pp 1125–1151

Horton P, Ruban AV, Rees D, Pascal AA, Noctor G, Young AJ (1991) Control of the light-harvesting function of chloroplast membranes by aggregation of the LHCII chlorophyll-protein complex. FEBS Lett **292:** 1–4

Humbeck K, Melis A, Krupinska K (1994) Effects of chilling on chloroplast development in barley primary foliage leaves. J Plant Physiol **143:** 744–749

Jansson S (1994) The light-harvesting chlorophyll a/b binding proteins. Biochim Biophys Acta **1184:** 1–19

Keefe D, Mets L (1983) Bundle sheath cell development in *Flaveria palmeri* (abstract no. 239). Plant Physiol **72:** S-43

Laetsch WM (1971) Chloroplast structural relationships in leaves of C_4 plants. *In* MD Hatch, CB Osmond, RO Slatyer, eds, Photosynthesis and Photorespiration. Wiley-Interscience, New York, pp 323–349

Leong T-Y, Anderson JM (1984) Adaptation of the thylakoid membranes of pea chloroplasts to light intensities. II. Regulation of electron transport capacities, electron carriers, coupling factor (CF_1) activity and rates of photosynthesis. Photosynth Res **5:** 117–128

Lichtenthaler HK (1987) Chlorophylls and carotenoids: pigments of photosynthetic biomembranes. Methods Enzymol **148:** 350–382

Liu Y, Dengler NG (1994) Bundle sheath and mesophyll cell differentiation in the C_4 dicotyledon *Atriplex rosea*: quantitative ultrastructure. Can J Bot **72:** 644–657

Mateu-Andrés I (1993) Micro-ecology and some related aspects of C_4 plants living in Europe. Photosynthetica **29:** 583–594

Mayne BC, Dee AM, Edwards GE (1974) Photosynthesis in mesophyll protoplasts and bundle sheath cells of various type of C_4 plants. III. Fluorescence emission spectra, delayed light emission, and P700 content. Z Pflanzenphysiol **74:** 275–291

Meierhoff K, Westhoff P (1993) Differential biogenesis of photosystem II in mesophyll and bundle-sheath cells of monocotyledonous NADP-malic enzyme-type C_4 plants: the non-stoichiometric abundance of the subunits of photosystem II in the bundle-sheath chloroplasts and the translational activity of the plastome-encoded genes. Planta **191:** 23–33

Meister A (1992) New fluorometric method for determination of chlorophyll *a*/*b* ratio. Photosynthetica **26:** 533–539

Melis A (1989) Spectroscopic methods in photosynthesis: photosystem stoichiometry and chlorophyll antenna size. Phil Trans R Soc Lond B **323:** 397–409

Melis A (1991) Dynamics of photosynthetic membrane composition and function. Biochim Biophys Acta **1058:** 87–106

Melis A, Spangfort M, Andersson B (1987) Light-absorption and electron-transport balance between photosystem II and photosystem I in spinach chloroplasts. Photochem Photobiol **45:** 129–136

Moore Bd, Ku MSB, Edwards GE (1984) Isolation of leaf bundle sheath protoplasts from C_4 dicot species and intracellular localization of selected enzymes. Plant Sci Lett **35:** 127–138

Moore Bd, Ku MSB, Edwards GE (1989) Expression of C_4-like photosynthesis in several species of *Flaveria*. Plant Cell Environ **12:** 541–549

Mukerji I, Sauer K (1990) A spectroscopy study of a photosystem I antenna complex. *In* M Baltcheffsky, ed, Current Research in Photosynthesis, Vol II. Kluwer Academic Publishers, Dordrecht, The Netherlands, pp 321–324

Peter GF, Thornber JP (1991) Electrophoretic procedures for fractionating of photosystem I and II pigment-proteins of higher plants and for determination of their subunit composition. Methods Plant Biochem **5:** 195–209

Pfündel E, Baake E (1990) A quantitative description of fluorescence excitation spectra in intact bean leaves greened under intermittent light. Photosynth Res **26:** 19–28

Pfündel E, Bilger W (1994) Regulation and possible function of the violaxanthin cycle. Photosynth Res **42:** 89–109

Pfündel E, Meister A (1996) Flow cytometry of mesophyll and bundle sheath chloroplasts of maize (*Zea mays* L.). Cytometry **23:** 97–105

Pyliotis NA, Woo KC, Downton WJS (1971) Thylakoid aggregation correlated with chlorophyll *a*/chlorophyll *b* ratio in some C_4 species. *In* MD Hatch, CB Osmond, RO Slatyer, eds, Photosynthesis and Photorespiration. Wiley-Interscience, New York, pp 406–412

Rijgersberg CP, Amesz, J, Thielen APGM, Swager JA (1979) Fluorescence emission spectra of chloroplasts and subchloroplast preparations at low temperature. Biochim Biophys Acta **545:** 473–482

Ruban AV, Young AJ, Pascal AA, Horton P (1994) The effects of illumination on the xanthophyll composition of the photosystem II light-harvesting complexes of spinach thylakoid membranes. Plant Physiol **104:** 227–234

Schuster G, Ohad I, Martineau B, Taylor WC (1985) Differentiation and development of bundle sheath and mesophyll thylakoids in maize. Thylakoid polypeptide composition, photophorylation, and organization of photosystem II. J Biol Chem **260:** 11866–11873

Siefermann-Harms D (1987) The light-harvesting and protective functions of carotenoids in photosynthetic membranes. Physiol Plant **69:** 561–568

Siefermann-Harms D, Ninnemann H (1982) Pigment organization in the light-harvesting chlorophyll-*a*/*b* protein complex of lettuce chloroplasts. Evidence obtained from protection of the chlorophylls against proton attack and from excitation energy transfer. Photochem Photobiol **35:** 719–731

Staehelin LA, Arntzen CL (1983) Regulation of chloroplast membrane function: protein phosphorylation changes the spatial organization of membrane components. J Cell Biol **97:** 1327–1337

Thayer SS, Björkman O (1992) Carotenoid distribution and deepoxidation in thylakoid pigment-protein complexes from cotton leaves and bundle-sheath cells of maize. Photosynth Res **33:** 213–225

Tjus SE, Roobol-Boza M, Pålsson LO, Andersson B (1995) Rapid isolation of photosystem I chlorophyll-binding proteins by anion exchange perfusion chromatography. Photosynth Res **46:** 339–345

Trissl H-W, Wilhelm C (1993) Why do thylakoid membranes from higher plants form grana stacks? Trends Biochem Sci **18:** 415–419

Vogelmann TC (1993) Plant tissue optics. Annu Rev Plant Physiol Plant Mol Biol **44:** 231–251

Walters RG, Horton P (1994) Acclimation of *Arabidopsis thaliana* to the light environment: changes in composition of the photosynthetic apparatus. Planta **195:** 248–256

Weis E (1985) Chlorophyll fluorescence at 77 K in intact leaves: characterization of a technique to eliminate artifacts related to self-absorption. Photosynth Res **6:** 73–86

Wild A, Höpfner M, Rühle W, Richter M (1986) Changes in the stoichiometry of photosystem II components as an adaptive response to high-light and low-light conditions during growth. Z Naturforsch **41c:** 597–603

Wittmershaus BP, Woolf VM, Vermaas WFJ (1992) Temperature dependence and polarization of fluorescence from photosystem I in the cyanobacteria *Synechocystis* sp. PCC 6803. Photosynth Res **31:** 75–87

Woo KC, Anderson JM, Boardman NK, Downton WJS, Osmond CB, Thorne SW (1970) Deficient photosystem II in agranal bundle sheath chloroplasts of C_4 plants. Proc Natl Acad Sci USA **67:** 18–25